Journal of Alloys and Compounds 515 (2012) 143–148

Contents lists available at SciVerse ScienceDirect

Journal of Alloys and Compounds

journal homepage: www.elsevier.com/locate/jallcom

Structural, optical, and magnetic properties of Co-doped ZnO nanorods fabricated by a facile solution route

Hongjing Hao, Mei Qin, Ping Li*

Provincial Key Laboratory of Inorganic Nanomaterials, School of Chemistry and Materials Science, Hebei Normal University, Shijiazhuang 050016, China

ARTICLE INFO

Article history:
Received 12 July 2011
Received in revised form
21 November 2011
Accepted 24 November 2011
Available online 2 December 2011

Keywords:
Nanostructures
Chemical synthesis
Optical properties
Magnetic properties

ABSTRACT

In this study, a facile two-step solution route is demonstrated for the fabrication of Co-doped ZnO nanorods with diverse doping levels. The combination of XRD, EDS, and XPS measurements reveals that Co ions are successfully incorporated into the ZnO matrix and exist in the host lattice under the 2+ valence state. The substitution of Co^{2+} for Zn^{2+} does not change the wurtzite structure of ZnO nanocrystals. Co^{2+} dopant inhibits the dissolution of the intermediate product, thus, allowing a relatively slow and uniform deposition of the effective ions on the growing tiny rods. As a consequence, the obtained ZnO nanorods become longer and thinner with the increase in dopant concentration. Homogeneous substitutional doping is further verified by UV–vis absorption and photoluminescence spectroscopy. An obvious redshift in the wavelength of the absorption edge is observed in the doped ZnO samples, which can be attributed to the sp–d exchange interactions between the electrons in the conduction band of ZnO and the localized d electrons of the Co^{2+} cations. A remarkable quenching of yellow-green luminescence that results from doping is explained by an energy transfer mechanism. Furthermore, the doped ZnO exhibits room-temperature ferromagnetism, which is greatly suppressed and replaced by paramagnetism at higher doping levels.

1. Introduction

With a wide band gap of 3.37 eV and a large exciton binding energy of 60 meV, ZnO semiconductor has attracted a great deal of attention in the material research field. Due to its significant optical and electronic properties, ZnO has been widely used for fabricating various nano-optoelectronic devices [1–4]. Over the past few years, the doping of well-chosen impurities has been extensively explored as an effective technique to modify the properties of ZnO nanostructures [5–9]. Transition metal doping of ZnO has become an active research field ever since it was predicted to improve the optical and electronic properties of the oxide material, and particularly, lead to room-temperature ferromagnetism. Among these, the element of Co is considered a potential candidate for incorporating into ZnO because of its abundant electron states and large solubility in the ZnO matrix [10].

In recent years, many groups have synthesized Co-doped ZnO (Co:ZnO) nanostructures and studied the altered performance upon doping. For instance, Jones and coworkers [11] fabricated Co:ZnO submicrometer tubes using a polymer based template approach. They observed a 25-nm redshift in UV–vis absorption, which originated from the narrowing of the ZnO band gap (3.22 eV) as a result of Co doping. Wang's group [12] synthesized Co:ZnO nanorod arrays on a glass substrate via a solution route. They found that Co doping can effectively adjust the energy level in ZnO nanorods, lead to variation in the UV emission peak position, and enhance the luminescence performance in the visible light region. Bahadur's group [13] synthesized uniform and transparent $Zn_{1-x}Co_xO$ films by a sol–gel spin coating technique, and revealed that an increase in Co content in the range $0 \leq x \leq 0.10$ led to a decrease in band gap energy as well as quenching of the near band edge and blue emissions. Sharma et al. [14] prepared Co:ZnO nanoparticles by a co-precipitation technique. The obtained samples showed strong ferromagnetic behavior at room temperature. However, at higher doping levels, the ferromagnetic behavior was suppressed and the antiferromagnetic nature was enhanced. Xu and Cao [15] reported a hydrothermal method to synthesize $Zn_{1-x}Co_xO$ flakes, and found that the samples exhibited obvious ferromagnetic characteristics at room temperature. Moreover, with more doping content of Co^{2+}, the ferromagnetic behavior was suppressed and paramagnetic nature was observed.

Previous studies have obviously demonstrated that the physical and chemical properties of the synthesized Co:ZnO samples are strongly sensitive to its preparative conditions [12,13]. Recently, much effort has been made to investigate wet chemical methods

* Corresponding author at: 113 Yuhua Road, Shijiazhuang 050016, Hebei, China. Tel.: +86 311 86268342.
E-mail address: lipingchina@yahoo.com.cn (P. Li).

0925-8388/$ – see front matter © 2011 Elsevier B.V. All rights reserved.
doi:10.1016/j.jallcom.2011.11.112

for the synthesis of metal-ion-doped ZnO nanostructures, including the sol–gel method [16,17] and various hydrothermal methods [18,19]. These direct synthetic methods can allow a better control over chemical composition and dopant incorporation. Here, a two-step solution route is reported to synthesize homogeneous Co:ZnO nanorods at a low temperature (100 °C) with no assisted template. The diversification caused by Co doping on structural, morphological, optical, and magnetic properties of ZnO was discussed in detail. Our results indicate that the current doping process is a potential method to produce high quality transition metal-doped ZnO nanocrystals with adjustable properties.

2. Experimental

2.1. Preparation of pure ZnO and Co:ZnO nanorods

All reagents employed in these experiments, including zinc chloride ($ZnCl_2$, ≥98.0%), cobalt chloride ($CoCl_2$, ≥98.0%), and sodium hydroxide (NaOH, ≥96.0%), were purchased from Tianjin Chemical Reagent Company. They were of analytical grade and have been used without further purification. The reagents were dissolved in deionized water at room temperature to obtain the standard solutions of 1.0, 0.1, and 4.0 M, respectively, prior to the synthetic experiments. Pure ZnO and Co:ZnO nanorods were prepared using a facile two-step solution method as described in the following: 20 mL of the $ZnCl_2$ solution was mixed with different volumes of the $CoCl_2$ solution under vigorous stirring, according to the required Co doping levels. Then, 45 mL of the NaOH solution was added dropwise to the above mixture with water added to reach a volume of 100 mL of clear solution ($[Zn^{2+}] = 0.2$ M, $[OH^-] = 1.8$ M; molar ratio of $Zn^{2+}/OH^- = 1:9$). Co doping levels were defined as 0, 3, 5, 8, and 10 mol% by altering the injection volume of the $CoCl_2$ solution (0, 6, 10, 16, and 20 mL). The above primary precursor was maintained with mild, continuous stirring at 40 °C for 1.5 h. Subsequently, the precursor after pre-stirring was transferred to a 250-mL conical flask and heated at normal atmospheric pressure (1 atm). When it reaches its boiling point after ca. 30 min, the mixture was refluxed for an additional 5 h. After this reaction, the precipitate was filtered, thoroughly rinsed, and air-dried at ambient temperature.

2.2. Characterization

The crystallinity and phase purity of the as-prepared samples were investigated using a Bruker-AXS D8 ADVANCE X-ray diffractometer (XRD; Cu Kα radiation, λ = 0.15406 nm). The morphologies of the crystals were observed on a HITACHI S-4800 field emission scanning electron microscopy (FESEM). The energy-dispersive spectrometer (EDS; OXFORD INCA ENERGY 350) together with X-ray photoelectron spectroscopy (XPS; PHI-5702) were used to confirm the dopant content and the chemical bonding states of Co ions in the Co:ZnO nanorods. The optical absorption spectra were recorded with a SHIMADZU UV-2501PC UV-VIS spectrophotometer. Photoluminescence (PL) spectra were determined at room temperature with a HITACHI F-4500 spectroscopy using Xe laser as an excitation source. The magnetic properties of the doped samples were characterized using a Quantum Design MODEL 6000 Physical Property Measurement System.

3. Results and discussion

3.1. XRD analysis of ZnO samples

XRD measurements on pure ZnO and Co:ZnO nanorods are presented in Fig. 1. The spectra reveal that all the samples are highly crystallized, which can be identified by their sharp and intense peaks. The main diffraction peaks are in good agreement with the hexagonal wurtzite structure of ZnO (JCPDS No. 36-1451). No characteristic peaks of metallic cobalt, cobalt oxides (i.e., CoO and Co_2O_3), and other compounds are detected in 3 mol% and 5 mol% Co:ZnO samples, suggesting that the doped Co ions are primarily incorporated into the ZnO lattice. However, the impurity phase of $Co(OH)_2$ (indicated with an asterisk) begins to appear in the Co:ZnO samples with 8 mol% and 10 mol% doping levels. Semiquantitative analysis of the crystal composition (mass%) reveals that the impurity content is about 5% and 8%, respectively, for the two samples. The $Co(OH)_2$ formation is regarded to be induced by the more dopant ions. Under these conditions, some of the Co ions contribute to forming $Co(OH)_2$ instead of incorporating into the zinc precursors in the initial hydrothermal solution. The lattice parameters were calculated using the TopasP-2 software attached on the XRD

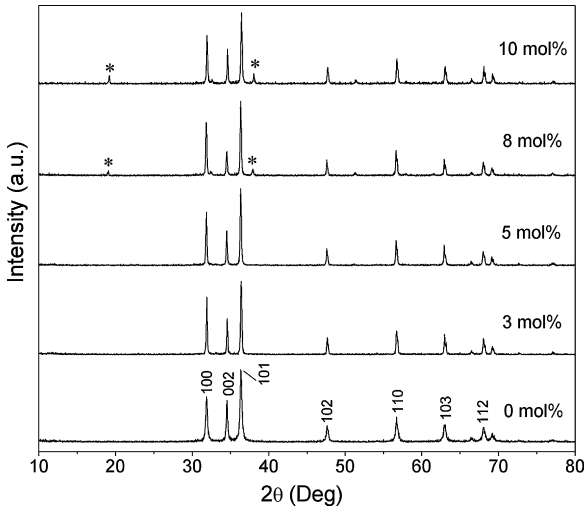

Fig. 1. XRD patterns of the ZnO nanocrystals that are doped with different levels of Co. The Co doping levels are indicated alongside.

Table 1
Calculated values of lattice parameters of the ZnO nanocrystals that are doped with different levels of Co.

Co-doping level (mol%)	Lattice parameter $a = b$ (Å)	Lattice parameter c (Å)
0	3.2539	5.2114
3	3.2490	5.2042
5	3.2442	5.1989

diffractometer. The resulting data are listed in Table 1. As shown in the table, Co doping slightly decreases the lattice parameters of ZnO nanocrystals. This change also suggests that most of the Co ions with smaller ionic radii substitute for Zn ions in the ZnO lattice, and the unit cell contracts to accommodate these heterogeneous ions.

3.2. Component analysis of ZnO samples

To investigate Co content and its distribution in the Co:ZnO nanocrystals, all the samples were subject to EDS determination. The obtained spectra are displayed in Fig. 2. Some weak Co-related peaks are present in the doped samples in addition to the obvious Zn and O peaks. Since Co dopant did not change the wurtzite structure of ZnO as identified by the XRD results, Co ions are successfully incorporated into the crystal structure of ZnO nanocrystals. Quantitative analysis of the atomic concentration (atom%) is listed in Table 2. The relative error of

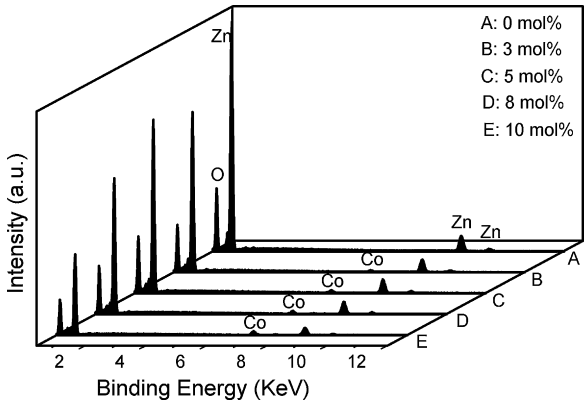

Fig. 2. EDS spectra of the ZnO nanocrystals that are doped with different levels of Co. The Co doping levels are indicated alongside.

Table 2
The composition of the ZnO nanocrystals dependence on Co-doping level.

Composition (atom %)	Co-doping level (mol%)				
	0	3	5	8	10
Zn	50.00	47.56	46.65	45.26	42.08
Co	0	2.44	3.35	4.74	7.92
O	50.00	50.00	50.00	50.00	50.00

accuracy is less than ±2%. The Co content in the samples changes from 2.44% (3 mol% Co:ZnO) to 7.92% (10 mol% Co:ZnO) with the increasing doping levels. However, the Co content determined from the EDS analysis (7.92%) in the 10 mol% Co:ZnO sample is much higher than that estimated from the XRD analysis (3.01%) of the same sample, indicating that most of the Co ions exist in Co:ZnO nanorods rather than in the $Co(OH)_2$. In addition, less Co is found in the Co:ZnO crystals than that provided in the precursor solution, which suggests the hindering of dopant incorporation into the ZnO lattice.

3.3. Chemical bonding states of doped Co ions

To confirm further the chemical bonding states of Co ions in the doped ZnO, XPS measurements were carried out on the samples. Fig. 3 shows the high resolution Co 2p spectrum of 5 mol% Co:ZnO sample. There are two main peaks, positioned at the binding energy sites of 781.0 eV and 797.5 eV, corresponding to the Co $2p_{3/2}$ and Co $2p_{1/2}$ orbitals, respectively. Simultaneously, two shake-up satellites of the main peaks are present at slightly higher energies. The satellite peak at a binding energy of about 6 eV higher than the main Co $2p_{3/2}$ peak is usually considered a feature of Co^{2+} ions [20]. Furthermore, a report stated that the Co $2p_{3/2}$ peak corresponding to the Co—Co bonding was located at 778.1–778.3 eV, and the peak corresponding to the Co—O bonding was located around 780 eV [21]. Therefore, Co clusters can be ruled out in the doped samples. Thus, Co ions, in the +2 oxidation state, are surrounded by O ions, that is, Co^{2+} successfully substitute for Zn^{2+} in the ZnO lattice.

3.4. Morphologies of ZnO nanocrystals

The general morphologies of ZnO samples are illustrated in Fig. 4. As observed in the figures, most of the pure ZnO have irregular appearances with only a small section of branched nanorods, and that all the Co:ZnO samples exhibit well-defined, uniform

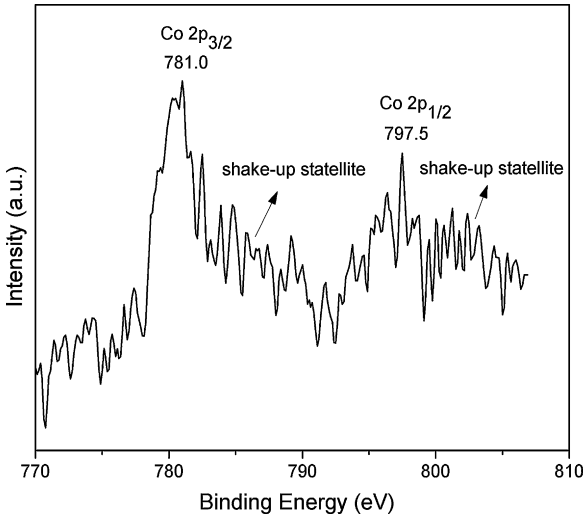

Fig. 3. XPS spectrum of Co 2p recorded from 5 mol% Co:ZnO sample.

nanorods. Concentrating on the doped ZnO with increasing Co content, the length of the nanorods increases from 1.2 μm to 1.8 μm accompanied with a mean diameter decreasing from 230 nm to 160 nm, which leads to a larger aspect ratio.

In the two-step synthesis process, the pre-stirring step is essential for the growth of ZnO nanorods, as it yields an intermediate product of $Zn(OH)_2$, which serves as a reservoir and slowly releases Zn^{2+} ions to allow the nucleation and growth for ZnO [22]. With the thermodynamical barrier induced by the addition of Co^{2+} ions [23], the nucleation, as well as the growth rate of the primary nuclei, slows down. The effective ions have more time to deposit uniformly on the nuclei along the *c*-axis. Thus, the aspect ratio of the Co:ZnO nanorods increases, and the surface of the nanorods becomes smoother with more dopant incorporation. Meanwhile, in the synthesis of pure ZnO, the intermediate $Zn(OH)_2$ dissolves rapidly due to the relatively low energy barrier, resulting in a high concentration of Zn^{2+} ions in the precursor. The saturation of the solution goes above the concentration for the nucleation of ZnO. It cannot allow the suitable growth of an individual nanorod instead, irregular or branched crystals are formed.

3.5. Absorption properties of ZnO nanocrystals

Absorption properties of ZnO samples were investigated to reveal the influence of Co doping on the energy band structure of ZnO. The testing wavelength ranges from 200 nm to 800 nm. Fig. 5 presents the UV–vis absorption spectra of pure and doped ZnO samples. The absorption onset of the doped ZnO shows an apparent redshift compared with the pure ZnO. The optical band gap energy of each sample was determined from the wavelength of the absorption edges. The energy curve versus Co doping level (see inset plot in Fig. 5) reveals a declining trend (from 3.09 eV to 2.63 eV) with the increasing doping concentration. The energy decrease is attributed to the sp–d exchange interactions between the s, p electrons in the conduction band of ZnO and the localized d electrons of the doped Co^{2+} cations. Based on the XRD patterns of 3 mol% and 5 mol% Co:ZnO (there is no secondary phase except ZnO), the above phenomenon is suggested to be probably the result from the substitutional Co^{2+} ions. Furthermore, the doped samples show three additional absorption bands at about 562, 609, and 660 nm. This feature is derived from the d–d electron transitions resulting from the tetrahedrally coordinated Co^{2+} in the ZnO wurtzite structure, and correspond to the $^4A_2(F)\rightarrow{}^2A_1(G)$, $^4A_2(F)\rightarrow{}^4T_1(P)$, and $^4A_2(F)\rightarrow{}^2E(G)$ transitions, respectively, in the high spin state of Co^{2+} [24]. Thus, the successful substitution of Co^{2+} for Zn^{2+} in the hexagonal ZnO wurtzite structure is confirmed.

3.6. Photoluminescence properties of ZnO nanocrystals

Fig. 6 presents the photoluminescence spectra of pure and doped ZnO. All the samples exhibit a strong UV emission at ~380 nm and a weak blue luminescence at ~450 nm. The pure ZnO also shows a yellow-green emission with its maximum at ~570 nm, but it is quenched in the doped samples. The UV emission is assigned to the band edge emission of ZnO host. The peak positions for Co:ZnO samples slightly shift to the longer wavelength in comparison with the pure ZnO (see inset plot in Fig. 6). This is due to the band gap narrowing of the ZnO nanocrystals with Co incorporation, as discussed in the previous section. A redshift phenomenon from pure ZnO to the doped samples occurs as well for the blue emission. The emission peak at ~450 nm is usually derived from the electron transition between the valence band and the shallow donor level formed by zinc interstitial defects [25]. The slight redshift of the peak results from the change in the acceptor level induced by the substitutional Co^{2+}. A remarkable difference shown between pure and doped ZnO lies in the quenching of yellow-green

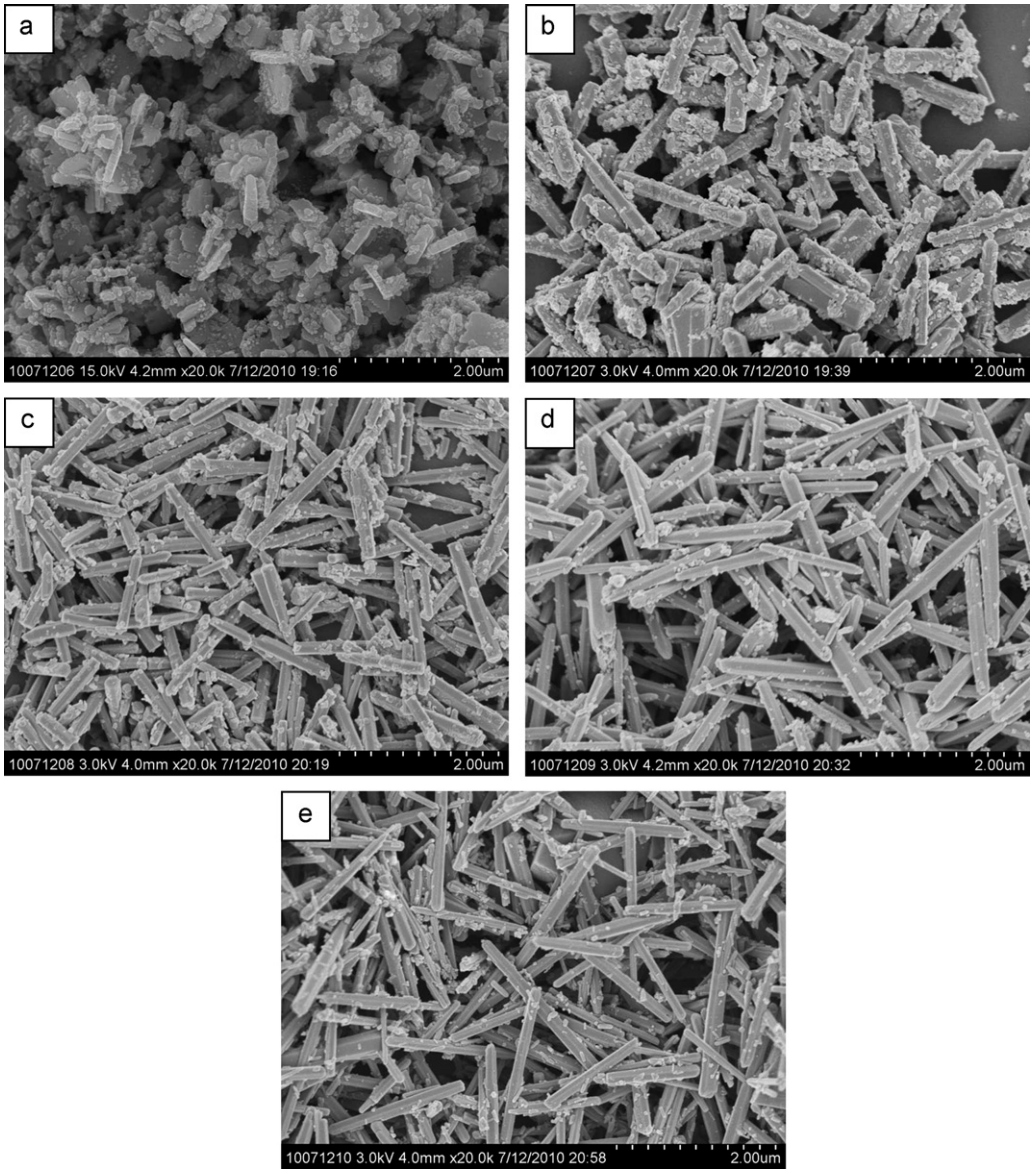

Fig. 4. FESEM images of the ZnO nanocrystals that are doped with different levels of Co: (a) 0 mol%, (b) 3 mol%, (c) 5 mol%, (d) 8 mol%, (e) 10 mol%.

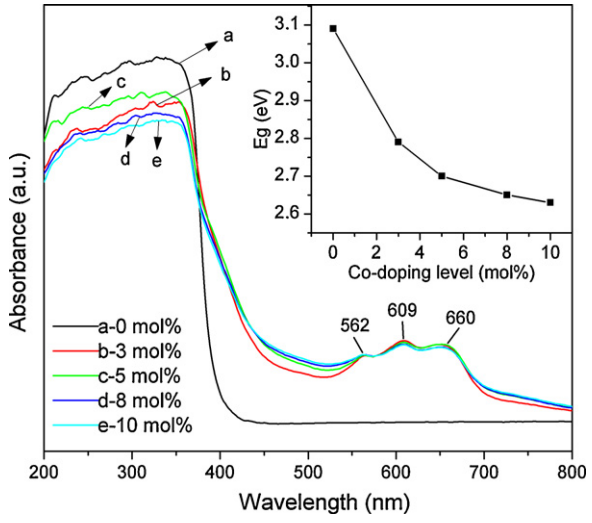

Fig. 5. UV–vis absorption spectra of the ZnO nanocrystals that are doped with different levels of Co.

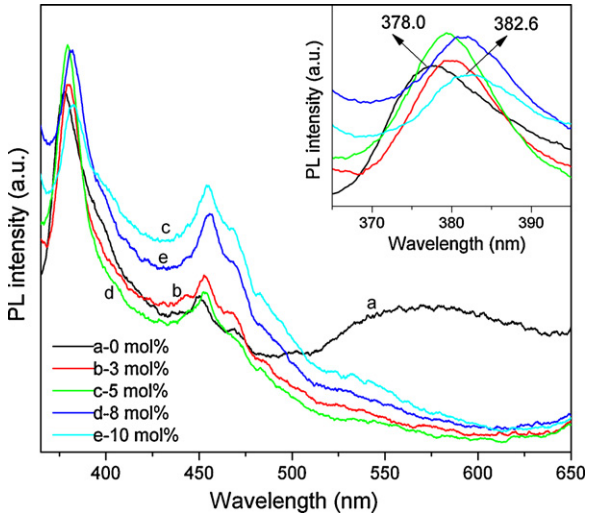

Fig. 6. Room-temperature PL spectra of the ZnO nanocrystals that are doped with different levels of Co.

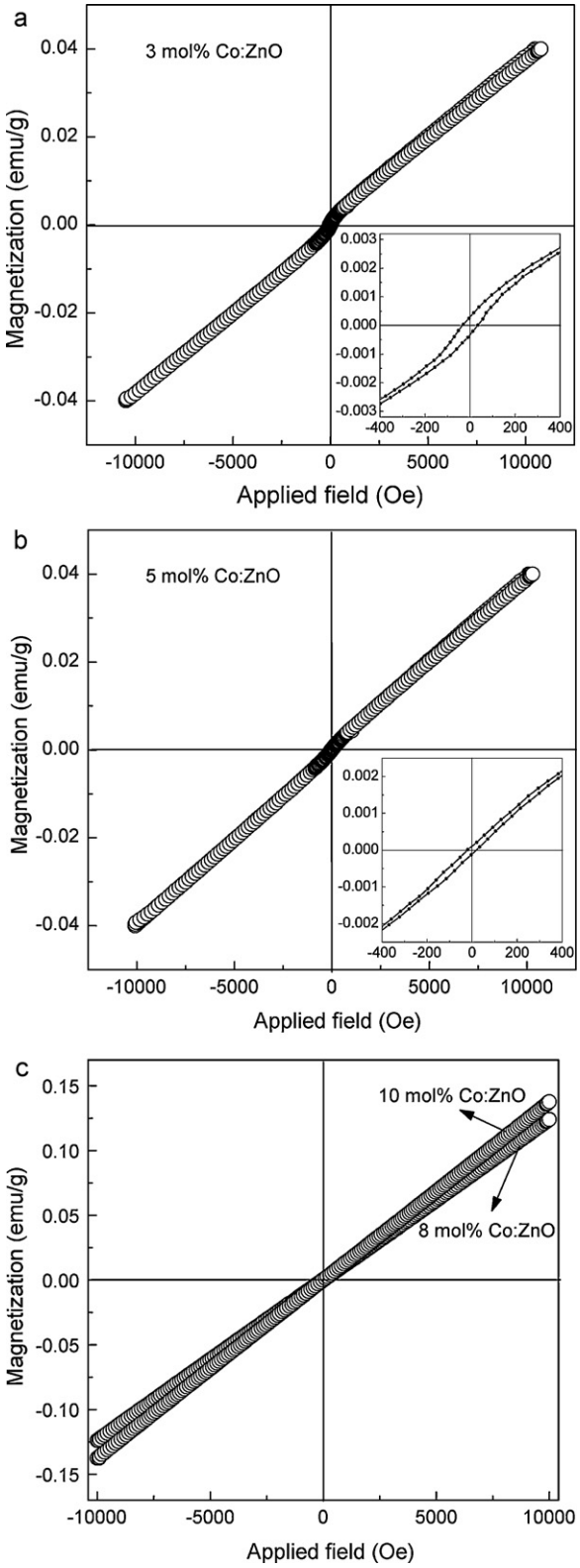

Fig. 7. Room-temperature M–H curves of the Co:ZnO nanorods that are doped with different levels of Co.

luminescence for all the Co:ZnO samples. This can be explained by the energy transfer mechanism [26,27]. The yellow-green luminescence of ZnO has been usually attributed to the electron transition from oxygen vacancies to the valence band of ZnO [28]. Comparing the luminescence spectra with the absorption spectra, the defect state energy (~2.17 eV) is very close to the photon energy (~2.20 eV), which resonantly excites the $^4A_2(F) \rightarrow {}^2A_1(G)$ transition of Co^{2+}. Therefore, the Co^{2+} in the ZnO lattice absorbs the energy from the defect emission, that is, the energy transferred from the defect emission to the electron transition of Co^{2+}. Thus, this results in the quenching of the yellow-green luminescence in the Co:ZnO nanocrystals.

3.7. Magnetic properties of ZnO nanocrystals

The magnetic properties of the doped ZnO were measured at room temperature (300 K). Fig. 7 shows the dependence of magnetization with the applied magnetic field (M–H curves). The 3 mol% and 5 mol% Co:ZnO samples show weak ferromagnetism at lower field values and paramagnetism at higher field values. The hysteresis loops for the two samples shown in Fig. 7(a) and (b) present with the coercivity (Hc) values 40 Oe and 25 Oe, respectively, and the remnant magnetization (Mr) values 3.6E−4 emu/g and 1.5E−4 emu/g, respectively, revealing that the latter sample with more Co content exhibits a weaker ferromagnetism than the former. When the Co doping level increased up to 8 mol%, the doped samples show linear magnetization curves with no hysteresis visible within the applied field (see Fig. 7(c)), which can be identified as paramagnetism.

Concerning Co-related materials, only metallic Co exhibits high temperature ferromagnetism (T_c = 1400 K) [29,30]. However, the secondary phase of Co metal clusters has been ruled out by the XRD and XPS results in this work. Thus, the observed ferromagnetism at room temperature is suggested to be an intrinsic nature of the Co:ZnO nanocrystals. The concept of bound magnetic polarons (BMPs) in connection with magnetic semiconductors can be introduced here to explain the origin of the ferromagnetism [31,32]. In the current experiment, the doping of Co impurity produced a number of oxygen vacancies and/or interstitial zinc that may act as shallow donor electrons and form BMPs. The overlapping of the polarons created a spin-split impurity band, which can mediate the Co—Co coupling in a ferromagnetism way, and thus, resulted in the ferromagnetic behavior of the sample. As Co dopant increased, it is more probable for the doped Co^{2+} cations to occupy the next-nearest lattice sites. The nearest Co—Co pairs then coupled in an antiferromagnetic way [14] and suppressed the magnetization [33]. Thus, weaker ferromagnetism in 5 mol% Co:ZnO is observed compared to the 3 mol% sample. As more and more nearest Co—Co pairs exhibited antiferromagnetic interaction, the hysteresis loops disappear in the 8 mol% and 10 mol% Co:ZnO samples, which makes the highly Co-doped ZnO samples behave paramagnetism under the external applied field.

4. Conclusions

Pure ZnO and Co:ZnO nanorods are successfully synthesized using a facile two-step solution route. The doped Co ions, in the oxidation state of Co^{2+}, substitute for Zn^{2+} ions in the ZnO lattice without changing its wurtzite structure. The dopant content varies from 2.44% to 7.92% based on Co doping level. With the increasing Co content, the obtained ZnO nanorods become longer and thinner, which leads to a gradually increasing aspect ratio. The band gap energy of the samples decreases from 3.09 eV (pure ZnO) to 2.63 eV (10 mol% Co:ZnO), indicating that Co doping has a crucial influence on the energy band structure of ZnO. Both the UV emission and the blue luminescence show a redshift that originated from the narrowing of the band gap as a result of Co doping. The yellow-green luminescence is quenched in the doped ZnO samples, which may be caused by the energy transfer from the defect emission to the electron transition of Co^{2+}. Furthermore, the doped ZnO samples

exhibit weak ferromagnetic characteristics at room temperature, and with more doping content of Co^{2+}, the ferromagnetic behavior is greatly suppressed and paramagnetic nature is observed.

Acknowledgements

This work was supported by grants from Key Programs of Science and Technology Research of Ministry of Education of China (210020), the Key Project in Applied Basic Research of Hebei Province (09963537D), and Science Foundation of Hebei Normal University (L2007B13, L2008Z09). The use of the English language in this paper has been improved by ShineWrite.com Professional Editing Support.

References

[1] H.M. Yang, S. Nie, Mater. Chem. Phys. 114 (2009) 279–282.
[2] M. Yang, Z.X. Guo, K.H. Qiu, J.P. Long, G.F. Yin, D.G. Guan, S.T. Liu, S.J. Zhou, Appl. Surf. Sci. 256 (2010) 4201–4205.
[3] S.S. Lin, J.H. Song, Y.F. Lu, Z.L. Wang, Nanotechnology 20 (2009) 365703.
[4] M. Krunks, A. Katerski, T. Dedova, I.O. Acik, A. Mere, Sol. Energy Mater. Sol. Cells 92 (2008) 1016–1019.
[5] S. Rasouli, S.J. Moeen, J. Alloys Compd. 509 (2011) 1915–1919.
[6] J.B. Cui, Y.C. Soo, T.P. Chen, J. Phys. Chem. C 112 (2008) 4475–4479.
[7] Z. Sofer, D. Sedmidubský, Š. Huber, J. Hejtmánek, M. Maryško, K. Jurek, M. Mikulics, J. Cryst. Growth 314 (2011) 123–128.
[8] X.R. Qu, D.C. Jia, Mater. Lett. 63 (2009) 412–414.
[9] Q. Chen, J.L. Wang, Chem. Phys. Lett. 474 (2009) 336–341.
[10] H.B. Carvalho, M.P.F. Godoy, R.W.D. Paes, M. Mir, A.O. Zevallos, F. Iikawa, M.J.S.P. Brasil, V.A. Chitta, W.B. Ferraz, M.A. Boselli, A.C.S. Sabioni, J. Appl. Phys. 108 (2010) 033914.
[11] F. Ochanda, K. Cho, D. Andala, T.C. Keane, A. Atkinson, W.E. Jones, Langmuir 25 (2009) 7547–7552.
[12] B.Q. Wang, X.D. Shan, Q. Fu, J. Iqbal, Y. Lv, H.G. Fu, D.P. Yu, Physica E 41 (2009) 413–417.
[13] N. Bahadur, A.K. Srivastava, S. Kumar, M. Deepa, B. Nag, Thin Solid Films 518 (2010) 5257–5264.
[14] P.K. Sharma, R.K. Dutta, A.C. Pandey, J. Colloid Interface Sci. 345 (2010) 149–153.
[15] X.Y. Xu, C.B. Cao, J. Alloys Compd. 501 (2010) 265–268.
[16] J.H. Yang, L.Y. Zhao, X. Ding, L.L. Yang, Y.J. Zhang, Y.X. Wang, H.L. Liu, Mater. Sci. Eng. B 162 (2009) 143–146.
[17] M.E. Mercurio, A.W. Carbonari, M.R. Cordeiro, R.N. Saxena, L.Z. D'Agostino, J. Magn. Magn. Mater. 322 (2010) 1195–1197.
[18] X.L. Zhang, R. Qiao, J.C. Kim, Y.S. Kang, Cryst. Growth Des. 8 (2008) 2609–2613.
[19] A. Singhal, S.N. Achary, J. Manjanna, S. Chatterjee, P. Ayyub, A.K. Tyagi, J. Phys. Chem. C 114 (2010) 3422–3430.
[20] B.Q. Wang, C.H. Xia, J. Iqbal, N.J. Tang, Z.R. Sun, Y. Lv, L.N. Wu, Solid State Sci. 11 (2009) 1419–1422.
[21] Y.Z. Peng, T. Liew, W.D. Song, C.W. An, K.L. Teo, T.C. Chong, J. Supercond. Novel Magn. 18 (2005) 97–103.
[22] P. Li, H. Liu, F.X. Xu, Y. Wei, Mater. Chem. Phys. 112 (2008) 393–397.
[23] D.A. Schwartz, N.S. Norberg, Q.P. Nguyen, J.M. Parker, D.R. Gamelin, J. Am. Chem. Soc. 125 (2003) 13205–13218.
[24] H.A. Weakliem, J. Chem. Phys. 36 (1962) 2117–2141.
[25] H.B. Zeng, W.P. Cai, Y. Li, J.L. Hu, P.S. Liu, J. Phys. Chem. B 109 (2005) 18260–18266.
[26] M.Y. Zhong, G.Y. Shan, Y.J. Li, G.R. Wang, Y.C. Liu, Mater. Chem. Phys. 106 (2007) 305–309.
[27] D. Kouyate, J.C. Ronfard-Haret, P. Valat, J. Kossanyi, J. Lumin. 46 (1990) 329–337.
[28] J.S. Kang, H.S. Kang, S.S. Pang, E.S. Shim, S.Y. Lee, Thin Solid Films 443 (2003) 5–8.
[29] J.H. Kim, H. Kim, D. Kim, Y.E. Ihm, W.K. Choo, J. Appl. Phys. 92 (2002) 6066–6071.
[30] S. Kolesnik, B. Dabrowski, J. Mais, J. Appl. Phys. 95 (2004) 2582–2586.
[31] R. Janisch, P. Gopal, N.A. Spaldin, J. Phys.: Condens. Matter 17 (2005) R657–R689.
[32] J.M.D. Coey, M. Venkatesan, C.B. Fitzgerald, Nat. Mater. 4 (2005) 173–179.
[33] T. Bu1sgen, M. Hilgendorff, S. Irsen, F. Wilhelm, A. Rogalev, D. Goll, M. Giersig, J. Phys. Chem. C 112 (2008) 2412–2417.